

PAPER

Sampling-based Continuous Optimization for Messenger RNA Design

Feipeng Yue,¹ Ning Dai,¹ Wei Yu Tang,³ Tianshuo Zhou,¹ David Mathews^{4,5,6}, Liang Huang^{1,2,*}

¹School of EECS, Oregon State University, Corvallis, 97330, OR, USA, ²Dept. of Biochemistry & Biophysics, Oregon State University, Corvallis, 97330, OR, USA, ³Dept. of Quantitative and Computational Biology, University of Southern California, Los Angeles, 90089, CA, USA, ⁴Dept. of Biochemistry & Biophysics, University of Rochester Medical Center, Rochester, 14642, NY, 14642, ⁵Center for RNA Biology, University of Rochester Medical Center, Rochester, 14642, NY, 14642 and ⁶Dept. of Biostatistics & Computational Biology, University of Rochester Medical Center, Rochester, 14642, NY, 14642

Abstract

Designing messenger RNA (mRNA) sequences for a fixed target protein requires searching an exponentially large synonymous space while optimizing properties that affect stability and downstream performance. This is challenging because practical mRNA design involves multiple coupled objectives beyond classical folding criteria, and different applications prefer different trade-offs. We propose a general sampling-based continuous optimization framework, inspired by SamplingDesign, that iteratively samples candidate synonymous sequences, evaluates them with black-box metrics, and updates a parameterized sampling distribution. Across a diverse UniProt protein set and the SARS-CoV-2 spike protein, our method consistently improves the chosen objective, with particularly strong gains on average unpaired probability and accessible uridine percentage compared to LinearDesign and EnsembleDesign. Moreover, our multi-objective COMBO formulation enables weight-controlled exploration of the design space and naturally extends to incorporate additional computable metrics.

Key words: Messenger RNA, mRNA design, continuous optimization, sampling

1. Introduction

Designing optimized messenger RNA (mRNA) sequences has received increasing attention in recent years, driven in part by the success of mRNA vaccines during the COVID-19 pandemic (Baden *et al.*, 2021; Polack *et al.*, 2020). Given a target protein sequence, mRNA design seeks a synonymous coding sequence that preserves translation while optimizing desired mRNA properties. Because codon degeneracy creates an exponentially large set of synonymous sequences, exhaustive search is infeasible (Zhang *et al.*, 2023); effective methods must therefore navigate this space under explicitly defined objectives.

Several methods have demonstrated that large-scale optimization over synonymous spaces is feasible when objectives are clearly defined. LinearDesign optimized synonymous mRNAs under a minimum free energy (MFE) objective using dynamic programming, enabling efficient search at scale (Zhang *et al.*, 2023). More recently, EnsembleDesign (Dai *et al.*, 2025) and JAX-RNAfold (Krueger and Ward, 2025) optimized a

distribution-level objective, ensemble free energy (EFE), using continuous optimization, but with very different approaches (e.g., the former extended LinearDesign's lattice parsing framework while the latter did not). These approaches highlight the value of objective-driven optimization for navigating the vast synonymous coding space. However, practical mRNA design involves many objectives beyond MFE and EFE, and different applications often require different trade-offs. One example is the average unpaired probability (AUP), which summarizes expected unpairedness across the transcript and is often used as a proxy related to degradation (Leppek *et al.*, 2022). Another example is accessible uridine percentage (accessible U% / AccessU), which we introduce in this work as a user-defined objective that measures the fraction of uridines that are structurally accessible (i.e., more likely to be unpaired). These considerations motivate a more general optimization framework that can directly optimize diverse objectives, rather than focusing on a small set of classical targets.

Motivated by this gap, we propose a general-purpose framework for mRNA design based on sampling-based continuous optimization. Our sampling-based optimization perspective is inspired by SamplingDesign, which demonstrates that continuous optimization coupled with Monte-Carlo sampling can be an effective paradigm for RNA design (Tang et al., 2026). Our method maintains a continuously parameterized sampling distribution over amino-acid-preserving nucleotide sequences and improves the distribution iteratively using samples scored by external evaluators. Concretely, each iteration draws candidate sequences from the current distribution, evaluates them under a chosen objective (for example, MFE, EFE, CAI, AUP, AccessU, or weighted combinations of multiple metrics such as COMBO), and updates the distribution parameters using sampling-based gradient estimates computed from the sampled sequences and their objective scores. This formulation supports optimizing both established objectives and additional potential mRNA evaluation objectives.

We evaluate on a diverse set of proteins from UniProt spanning a wide length range and on the SARS-CoV-2 spike protein as a representative long target, using a consistent scoring pipeline. Under single-metric optimization, our method consistently improves the targeted objective; most notably, when optimizing AUP or AccessU, our designed sequences achieve lower values than both LinearDesign and EnsembleDesign. Under COMBO optimization, our method enables weight-controlled navigation of the design space to obtain sequences that satisfy different optimization preferences. Importantly, because the optimization loop treats metrics as black-box evaluators of sampled sequences, the framework naturally extends to incorporate additional computable metrics beyond the current set, enabling richer objective combinations for future mRNA design tasks.

2. Preliminaries: mRNA Design for Protein

2.1. Protein Encoding in mRNA

Let $\mathbf{p} = (p_1, p_2, \dots, p_m)$ be a target protein sequence of length m , where each p_i is an amino acid. Let $\mathcal{N} \triangleq \{\text{A, C, G, U}\}$ denote the RNA nucleotide alphabet. An mRNA coding sequence is a nucleotide string $\mathbf{x} = (x_1, x_2, \dots, x_N) \in \mathcal{N}^N$, where $x_i \in \mathcal{N}$ and $N = 3m$.

Partition \mathbf{x} into m consecutive codons (triplets) in \mathcal{N}^3 . Under the standard genetic code, each codon maps to an amino acid (or a stop signal); concatenating the resulting amino acids yields a protein sequence. We say that \mathbf{x} encodes \mathbf{p} if this translation yields \mathbf{p} . Since multiple codons can map to the same amino acid, there are typically many distinct mRNA sequences that encode the same protein. Accordingly, our design space consists of synonymous coding sequences for \mathbf{p} : all candidates encode \mathbf{p} but may differ at the nucleotide level.

2.2. mRNA Design Problem

Given a fixed target protein sequence \mathbf{p} , mRNA design seeks a coding sequence \mathbf{x} that encodes \mathbf{p} while optimizing sequence-level properties measured by computable metrics.

Design space. We define the synonymous design space for \mathbf{p} as

$$\mathcal{X}(\mathbf{p}) \triangleq \left\{ \mathbf{x} \in \mathcal{N}^N : \text{translate}(\mathbf{x}) = \mathbf{p} \right\}, \quad (1)$$

i.e., the set of all mRNA coding sequences that translate to \mathbf{p} under the standard genetic code.

Objective. Although all $\mathbf{x} \in \mathcal{X}(\mathbf{p})$ encode the same protein, different synonymous choices can yield different properties relevant to downstream use. We assess a candidate by different computable metrics $g_1(\mathbf{x}, \mathbf{p}), \dots, g_k(\mathbf{x}, \mathbf{p})$, where $k \in \{1, \dots, K\}$. Because some metrics are to be maximized and others minimized, we map each raw metric to a direction-aligned term $f_k(\mathbf{x}, \mathbf{p})$ via a monotone transformation

$$f_k(\mathbf{x}, \mathbf{p}) \triangleq \phi_k(g_k(\mathbf{x}, \mathbf{p})), \quad (2)$$

so that smaller f_k always indicates a better score, i.e., better performance according to metric k .

We then optimize a scalar objective over $\mathcal{X}(\mathbf{p})$ using a normalized weighted sum of objective terms:

$$F(\mathbf{x}, \mathbf{p}) \triangleq \sum_{k=1}^K w_k f_k(\mathbf{x}, \mathbf{p}), \quad w_k \geq 0, \quad \sum_{k=1}^K w_k = 1. \quad (3)$$

When $K = 1$, this reduces to optimizing a single metric. The design problem is

$$\mathbf{x}^* \in \operatorname{argmin}_{\mathbf{x} \in \mathcal{X}(\mathbf{p})} F(\mathbf{x}, \mathbf{p}). \quad (4)$$

2.3. Sequence Optimization Metrics

For a fixed target protein \mathbf{p} , each candidate coding sequence $\mathbf{x} \in \mathcal{X}(\mathbf{p})$ encodes the same protein but can exhibit different sequence-level and structure-level behaviors relevant to downstream use. We therefore evaluate \mathbf{x} with several standard computable metrics.

Folding model and notation. RNA secondary-structure metrics are based on the standard thermodynamic view that a sequence \mathbf{x} can adopt many feasible secondary structures, each associated with an energy. Let $\mathcal{Y}(\mathbf{x})$ be the set of feasible secondary structures for \mathbf{x} under a chosen energy model, and let $\Delta G^\circ(\mathbf{x}, \mathbf{y})$ denote the Gibbs free energy of structure $\mathbf{y} \in \mathcal{Y}(\mathbf{x})$. We use thermodynamic parameters (R, T) , where R is the universal gas constant and T is temperature. Let $p_{i,j}(\mathbf{x})$ denote the marginal probability that positions (i, j) form a base pair in the Boltzmann ensemble, and define the unpaired probability of position i

$$q_i(\mathbf{x}) \triangleq 1 - \sum_{j \neq i} p_{i,j}(\mathbf{x}), \quad i = 1, \dots, N. \quad (5)$$

Minimum free energy (MFE). The minimum free energy summarizes the most stable (lowest-energy) structure:

$$\text{MFE}(\mathbf{x}) \triangleq \min_{\mathbf{y} \in \mathcal{Y}(\mathbf{x})} \Delta G^\circ(\mathbf{x}, \mathbf{y}). \quad (6)$$

We compute MFE using LinearFold (Huang et al., 2019) in this work.

Boltzmann ensemble and ensemble free energy (EFE). Rather than focusing on a single structure, the partition function aggregates contributions from all feasible structures, weighting each by its Boltzmann factor:

$$Q(\mathbf{x}) \triangleq \sum_{\mathbf{y} \in \mathcal{Y}(\mathbf{x})} \exp\left(-\frac{\Delta G^\circ(\mathbf{x}, \mathbf{y})}{RT}\right). \quad (7)$$

The corresponding ensemble free energy is

$$\text{EFE}(\mathbf{x}) \triangleq -RT \log Q(\mathbf{x}), \quad (8)$$

which we compute using LinearPartition (Zhang *et al.*, 2020) in this work.

Average unpaired probability (AUP). The average unpaired probability is

$$\text{AUP}(\mathbf{x}) \triangleq \frac{1}{N} \sum_{i=1}^N q_i(\mathbf{x}). \quad (9)$$

Accessible U% (AccessU). Accessible U% weights unpaired probabilities by whether the nucleotide is U:

$$\text{AccessU}(\mathbf{x}) \triangleq \frac{1}{N} \sum_{i=1}^N \mathbf{1}[x_i = \text{U}] q_i(\mathbf{x}). \quad (10)$$

Codon Adaptation Index (CAI). CAI measures synonymous codon-usage bias relative to a reference set of highly expressed genes, and is commonly used as a metric of codon optimality (Sharp and Li, 1987).

Combined objective (COMBO). To express trade-offs among multiple criteria, we combine direction-aligned terms in a normalized weighted sum. Since $\text{CAI}(\mathbf{x})$, $\text{AUP}(\mathbf{x})$, and $\text{AccessU}(\mathbf{x})$ lie in $[0, 1]$, they are directly comparable after aligning directions (maximized terms are converted to minimization by $1 - \cdot$). In contrast, $\text{MFE}(\mathbf{x})$ is length-dependent; we therefore normalize it using a fixed baseline sequence for the same target protein. Let $\text{MFE}_{\text{LD}}(\mathbf{p})$ denote the MFE of the LinearDesign baseline sequence for \mathbf{p} . We use the normalized MFE score

$$\text{MFE}_{\text{rel}}(\mathbf{x}) \triangleq \frac{\text{MFE}(\mathbf{x})}{\text{MFE}_{\text{LD}}(\mathbf{p})}, \quad (11)$$

so that larger $\text{MFE}_{\text{rel}}(\mathbf{x})$ indicates a better (more stable) design relative to the baseline.

Putting these together, the combined objective is

$$\begin{aligned} \text{COMBO}(\mathbf{x}, \mathbf{p}) \triangleq & \alpha(1 - \text{CAI}(\mathbf{x})) + \beta \text{AUP}(\mathbf{x}) \\ & + \gamma \text{AccessU}(\mathbf{x}) + \delta(1 - \text{MFE}_{\text{rel}}(\mathbf{x})) \end{aligned} \quad (12)$$

where $\alpha, \beta, \gamma, \delta \geq 0$ and $\alpha + \beta + \gamma + \delta = 1$.

3. Parameterized Sampling Lattice for Synonymous mRNA Design

The synonymous design space $\mathcal{X}(\mathbf{p})$ is exponentially large and is defined by a hard amino-acid constraint. To avoid enumerating $\mathcal{X}(\mathbf{p})$ while preserving feasibility, we

represent it as a lattice and parameterize a sampling distribution directly on this structure (Fig. 1).

DFA lattice representation. Following LinearDesign, the set of coding sequences that encode a fixed target protein \mathbf{p} is compactly represented by a deterministic finite-state automaton (DFA) (Zhang *et al.*, 2023). In this lattice, each edge is labeled by a nucleotide, and any complete path generates an mRNA sequence $\mathbf{x} \in \mathcal{N}^N$ by concatenating edge labels. By construction, every complete path translates to \mathbf{p} , and conversely, every $\mathbf{x} \in \mathcal{X}(\mathbf{p})$ is represented by at least one complete path in the lattice. This DFA therefore provides a constraint-preserving representation of the synonymous space.

From a lattice to a sampling distribution. To enable continuous optimization in an otherwise discrete space, we follow the continuous relaxation perspective of EnsembleDesign and equip the same lattice with probabilistic parameters, yielding a probabilistic DFA (pDFA) that defines a distribution over synonymous sequences (Dai *et al.*, 2025). Crucially, probability mass is assigned only to valid DFA paths, so sampling from the pDFA produces sequences in $\mathcal{X}(\mathbf{p})$ automatically.

Formally, let s denote a lattice state and let $\mathcal{A}(s)$ be its set of outgoing edges. We associate each state with a categorical distribution over outgoing edges,

$$p_\theta(a | s) \geq 0, \quad \sum_{a \in \mathcal{A}(s)} p_\theta(a | s) = 1, \quad (13)$$

where θ collects all trainable parameters. Sampling corresponds to traversing the lattice by repeatedly selecting an outgoing edge $a \sim p_\theta(\cdot | s)$ and advancing to the next state. The resulting concatenation of edge labels yields a sampled $\mathbf{x} \sim p_\theta(\cdot)$ supported on $\mathcal{X}(\mathbf{p})$.

Parameterized local transitions. Rather than optimizing probabilities directly on the simplex, we introduce unconstrained logits $\theta_{s,a} \in \mathbb{R}$ for each $a \in \mathcal{A}(s)$. Local transition probabilities are obtained via the softmax,

$$p_\theta(a | s) = \frac{\exp(\theta_{s,a})}{\sum_{a' \in \mathcal{A}(s)} \exp(\theta_{s,a'})}, \quad a \in \mathcal{A}(s), \quad (14)$$

which automatically enforces nonnegativity and normalization while allowing updates to be performed in an unconstrained Euclidean space.

Sequence probability and path factorization. A sampled sequence \mathbf{x} corresponds to a complete path $\tau = (s_0, a_0, \dots, s_{N-1}, a_{N-1}, s_N)$ on the lattice, where a_n denotes the chosen outgoing edge at state s_n . Under (14), the probability of sampling the path (and thus the sequence) factorizes along the path:

$$p_\theta(\mathbf{x}) = p_\theta(\tau) = \prod_{n=0}^{N-1} p_\theta(a_n | s_n). \quad (15)$$

Equivalently,

$$\log p_\theta(\mathbf{x}) = \sum_{n=0}^{N-1} \log p_\theta(a_n | s_n). \quad (16)$$

This factorization is central to our approach. Our objective $\text{COMBO}(\mathbf{x}, \mathbf{p})$ is evaluated on discrete sequences

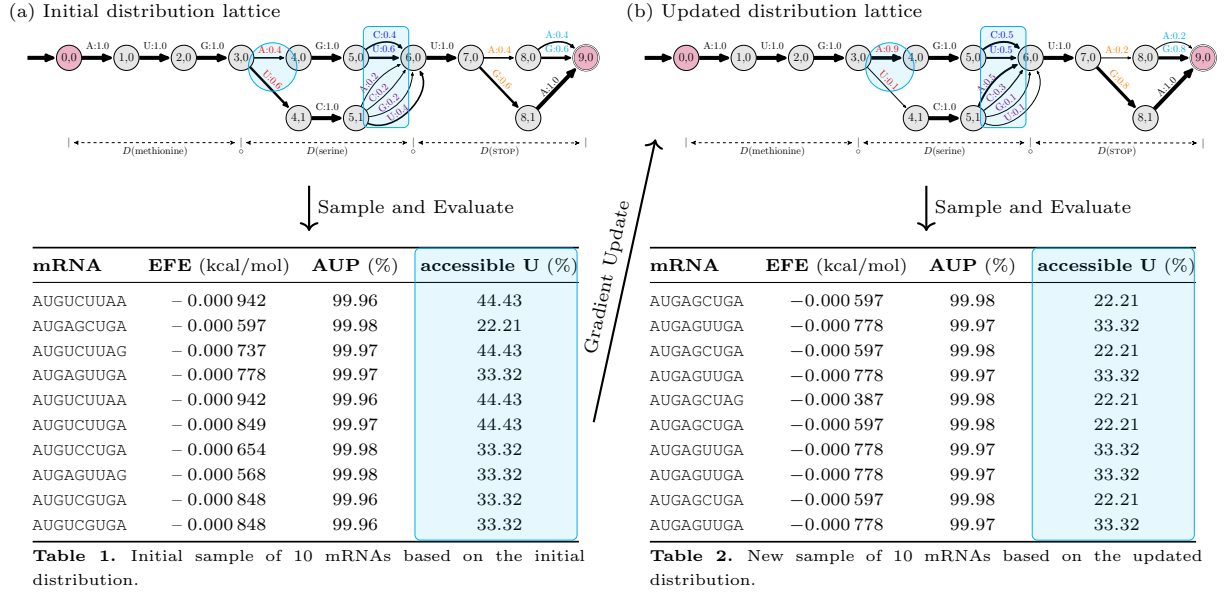


Fig. 1. The parameterized sampling lattice and an illustrative update-sample-evaluate iteration. (a–b) parameterized sampling lattice. To avoid enumerating the exponentially large synonymous space for a fixed protein \mathbf{p} , we represent all valid coding sequences as a DFA-based lattice, where each complete path corresponds to a synonymous mRNA \mathbf{x} . We then equip the lattice with probabilistic parameters, forming a pDFA in which each state defines a locally normalized distribution over its outgoing edges (Eq. 13). Edge labels are nucleotides, and sampling generates an mRNA by traversing the lattice and concatenating the emitted labels. **Illustrative workflow.** Starting from an initialized lattice (a), we sample candidate mRNAs and Evaluate them under the chosen objective (here, minimizing accessible U%). Using these scores, we perform a gradient update on the lattice parameters, yielding an updated probabilistic lattice (b), from which we sample and evaluate again. After the update, the sampled sequences exhibit a clear reduction in accessible U% (as highlighted by the cyan regions in the table), and the corresponding decision region shifts probability mass away from U-emitting branches (as highlighted by the cyan regions in the pDFA), consistent with reducing U-rich choices as one effective route to lowering accessible U%. This update-sample-evaluate loop is repeated until the optimization metrics converge.

using folding-based metrics and is treated as a black-box function of \mathbf{x} . Although COMBO is not differentiable with respect to nucleotide identities, the pDFA provides a differentiable handle through $\log p_{\theta}(\mathbf{x})$. In the next section, we leverage (16) to derive sampling-based gradient estimates and implement a sample-evaluate-update procedure to optimize θ .

4. Sampling-Based Continuous Optimization on the Lattice

In this section, we present our sampling-based continuous optimization algorithm for synonymous mRNA design. The method iterates a sample-evaluate-update loop on the parameterized sampling lattice, using a score-function gradient estimator in logit space and terminating via an early-stopping rule.

4.1. Sampling

Starting from the initial state, a candidate sequence \mathbf{x} is generated by traversing the lattice and repeatedly sampling an outgoing edge $a_n \sim p_{\theta}(\cdot | s_n)$. Concatenating the nucleotide labels along the sampled path yields $\mathbf{x} \in \mathcal{N}^N$. For each sampled \mathbf{x} , we record the corresponding lattice path $\tau = (s_0, a_0, \dots, s_{N-1}, a_{N-1}, s_N)$, where a_n is the chosen outgoing edge at s_n .

4.2. Evaluation

Each sampled sequence \mathbf{x} is assigned a scalar objective value $F(\mathbf{x}, \mathbf{p})$, where $F(\mathbf{x}, \mathbf{p})$ is either a single metric or the weighted combination COMBO(\mathbf{x}, \mathbf{p}) defined in Section 2.3. These objective values provide the learning signal for updating θ .

4.3. Gradient-Based Update

The update step adjusts the lattice logits (and hence the induced sampling distribution) to reduce the expected objective under the current lattice distribution. We index optimization iterations by $t \in \{1, 2, \dots\}$, and let θ_t denote the lattice parameters used to sample the batch at iteration t (i.e., after $t - 1$ updates). At iteration t , we perform a gradient-based update

$$\theta_{t+1} = \theta_t - \eta \widehat{\nabla} J_t, \quad (17)$$

where $\widehat{\nabla} J_t$ is a stochastic estimate of $\nabla_{\theta} J(\theta_t; \mathbf{p})$ derived below and η is the learning rate. In practice, we use Adam to compute an adaptive update from $\widehat{\nabla} J_t$ (Paragraph (vii)).

(i) Expected objective under the lattice distribution. Fix a target protein \mathbf{p} . Sampling on the lattice induces a distribution $p_{\theta}(\mathbf{x})$ over synonymous coding sequences \mathbf{x} .

We minimize the expected objective

$$J(\boldsymbol{\theta}; \mathbf{p}) \triangleq \mathbb{E}_{\mathbf{x} \sim p_{\boldsymbol{\theta}}(\cdot)}[F(\mathbf{x}, \mathbf{p})]. \quad (18)$$

(ii) Score-function (log-derivative) gradient. Since \mathbf{x} is discrete, we differentiate (18) using the log-derivative trick:

$$\begin{aligned} \nabla_{\boldsymbol{\theta}} J(\boldsymbol{\theta}; \mathbf{p}) &= \nabla_{\boldsymbol{\theta}} \sum_{\mathbf{x}} p_{\boldsymbol{\theta}}(\mathbf{x}) F(\mathbf{x}, \mathbf{p}) \\ &= \sum_{\mathbf{x}} p_{\boldsymbol{\theta}}(\mathbf{x}) F(\mathbf{x}, \mathbf{p}) \nabla_{\boldsymbol{\theta}} \log p_{\boldsymbol{\theta}}(\mathbf{x}) \\ &= \mathbb{E}_{\mathbf{x} \sim p_{\boldsymbol{\theta}}(\cdot)}[F(\mathbf{x}, \mathbf{p}) \nabla_{\boldsymbol{\theta}} \log p_{\boldsymbol{\theta}}(\mathbf{x})]. \end{aligned} \quad (19)$$

With M i.i.d. samples $\mathbf{x}^{(1)}, \dots, \mathbf{x}^{(M)} \sim p_{\boldsymbol{\theta}}(\cdot)$, a Monte Carlo estimate of (19) is

$$\widehat{\nabla_{\boldsymbol{\theta}} J} = \frac{1}{M} \sum_{i=1}^M F(\mathbf{x}^{(i)}, \mathbf{p}) \nabla_{\boldsymbol{\theta}} \log p_{\boldsymbol{\theta}}(\mathbf{x}^{(i)}). \quad (20)$$

The remaining task is to express $\nabla_{\boldsymbol{\theta}} \log p_{\boldsymbol{\theta}}(\mathbf{x}^{(i)})$ in terms of local lattice decisions.

(iii) Path decomposition of the score term. Each sampled sequence \mathbf{x} corresponds to a complete lattice path $\tau = (s_0, a_0, \dots, s_{N-1}, a_{N-1}, s_N)$ of length N . By the path factorization in Section 3 (Eqs. (15)–(16)),

$$\nabla_{\boldsymbol{\theta}} \log p_{\boldsymbol{\theta}}(\mathbf{x}) = \sum_{n=0}^{N-1} \nabla_{\boldsymbol{\theta}} \log p_{\boldsymbol{\theta}}(a_n | s_n). \quad (21)$$

Substituting (21) into (20) reduces the global score term to a sum of local contributions along the sampled path.

(iv) Local softmax derivative. At each visited state s , the outgoing distribution over $\mathcal{A}(s)$ is parameterized by logits via the softmax in Eq. (14). Let $a \in \mathcal{A}(s)$ be the chosen edge on the sampled path, and let $u \in \mathcal{A}(s)$ index an arbitrary outgoing edge. Then

$$\frac{\partial}{\partial \theta_{s,u}} \log p_{\boldsymbol{\theta}}(a | s) = \mathbf{1}[u = a] - p_{\boldsymbol{\theta}}(u | s). \quad (22)$$

This provides an explicit per-logit local score term.

(v) Mean-variance normalization. For the batch scores $\{F(\mathbf{x}^{(i)}, \mathbf{p})\}_{i=1}^M$, we compute the batch mean and standard deviation

$$\begin{aligned} b &\triangleq \frac{1}{M} \sum_{i=1}^M F(\mathbf{x}^{(i)}, \mathbf{p}), \\ \sigma &\triangleq \sqrt{\frac{1}{M} \sum_{i=1}^M (F(\mathbf{x}^{(i)}, \mathbf{p}) - b)^2} + \varepsilon. \end{aligned} \quad (23)$$

and define the normalized weight

$$A^{(i)} \triangleq \frac{F(\mathbf{x}^{(i)}, \mathbf{p}) - b}{\sigma}. \quad (24)$$

Subtracting a baseline is a standard variance-reduction device for score-function gradient estimators (Williams, 1992; Greensmith *et al.*, 2004). Here we set b to the batch

mean so that each sample is weighted by its performance relative to the current batch rather than by the absolute scale of F .

(vi) Fully expanded per-logit gradient estimator.

Let the i -th sampled sequence have path $\tau^{(i)} = (s_0^{(i)}, a_0^{(i)}, \dots, s_{N-1}^{(i)}, a_{N-1}^{(i)}, s_N^{(i)})$. Combining (20), (21), and (22), for any state s and any $u \in \mathcal{A}(s)$,

$$\begin{aligned} \frac{\partial \widehat{J}(\boldsymbol{\theta}; \mathbf{p})}{\partial \theta_{s,u}} &= \frac{1}{M} \sum_{i=1}^M A^{(i)} \sum_{n=0}^{N-1} \mathbf{1}[s_n^{(i)} = s] \\ &\quad \cdot \left(\mathbf{1}[u = a_n^{(i)}] - p_{\boldsymbol{\theta}}(u | s) \right). \end{aligned} \quad (25)$$

The indicator $\mathbf{1}[s_n^{(i)} = s]$ ensures that only states visited by the sampled paths contribute to the corresponding logits.

(vii) Adam updates in logit space. Let $\widehat{\nabla J}_t$ denote the collection of all per-logit gradient estimates in (25) at iteration t . We use the Adam optimizer, which maintains exponential moving averages of past gradients and squared gradients to form a momentum term and an adaptive, per-parameter step size (Kingma and Ba, 2017). This is convenient for stochastic sampling-based gradient estimates and typically yields more stable updates than a fixed learning rate.

We update logits with Adam:

$$\begin{aligned} m_t &= \beta_1 m_{t-1} + (1 - \beta_1) \widehat{\nabla J}_t, \\ v_t &= \beta_2 v_{t-1} + (1 - \beta_2) \widehat{\nabla J}_t^2, \\ \hat{m}_t &= \frac{m_t}{1 - \beta_1^t}, \quad \hat{v}_t = \frac{v_t}{1 - \beta_2^t}, \\ \boldsymbol{\theta}_{t+1} &= \boldsymbol{\theta}_t - \eta \frac{\hat{m}_t}{\sqrt{\hat{v}_t} + \varepsilon}. \end{aligned} \quad (26)$$

4.4. Early Stopping and Termination Criteria

The sample-evaluate-update loop is stochastic and can be computationally expensive, as each iteration requires evaluating folding-based objectives on a batch of sequences. In practice, the optimization often converges to a stable region of the search space, after which additional iterations produce little or no improvement in the observed objective values while incurring substantial runtime. We therefore adopt an early stopping criterion that terminates the procedure once progress on the target objective has plateaued.

Best-so-far tracking. At iteration t , we draw a batch $\{\mathbf{x}^{(i)}\}_{i=1}^M \sim p_{\boldsymbol{\theta}_t}(\cdot)$ and compute their objective values $\{F(\mathbf{x}^{(i)}, \mathbf{p})\}_{i=1}^M$. Let the current best objective value in the batch be

$$(\widehat{F}_{\min})_t \triangleq \min_{i \in \{1, \dots, M\}} F(\mathbf{x}^{(i)}, \mathbf{p}), \quad (27)$$

and let the best value observed up to iteration t be updated by

$$F_t^* \triangleq \min(F_{t-1}^*, (\widehat{F}_{\min})_t), \quad F_0^* \triangleq +\infty. \quad (28)$$

Patience-based early stopping. We declare an iteration to be improving if it achieves a sufficient decrease relative

Algorithm 1 Sampling-based continuous optimization

```

1: Input: target protein  $\mathbf{p}$ , objective  $F(\cdot, \mathbf{p})$ , initialized
   lattice logits  $\theta_1$ 
2: Output: best sequence  $\mathbf{x}^*$ 
3: Initialize optimizer state;  $\mathbf{x}^* \leftarrow \emptyset$ ;  $F^* \leftarrow +\infty$ 
4: for  $t = 1, 2, \dots, T_{\max}$  do
5:   Sample a batch  $\{\mathbf{x}^{(i)}, \tau^{(i)}\}_{i=1}^M \sim p_{\theta_t}(\cdot)$ 
6:   Evaluate scores  $\{F(\mathbf{x}^{(i)}, \mathbf{p})\}_{i=1}^M$  and update  $\mathbf{x}^*, F^*$ 
7:   if early-stopping criterion is met then
8:     break
9:   end if
10:  Compute gradient estimate  $\widehat{\nabla J}_t$  and update logits
     to obtain  $\theta_{t+1}$ 
11: end for
12: return  $\mathbf{x}^*$ 

```

to the previous best:

$$F_t^* \leq F_{t-1}^* - \xi_{\text{stop}}. \quad (29)$$

Let P be a patience window (in iterations). We stop if no improving iteration occurs for P consecutive updates, i.e., if the number of iterations since the last improvement exceeds P .

Maximum-iteration safeguard. To bound runtime, we also impose a hard cap of T_{\max} iterations and stop once $t = T_{\max}$.

For convenience, Algorithm 1 provides a compact summary of the complete sample–evaluate–update procedure together with early stopping. Fig. 1 complements this summary with an illustrative example of how a single update shifts probability mass on the lattice and changes the resulting batch of samples.

5. Experimental Setup

5.1. Protein Targets

We evaluate on two groups of target proteins. The first group contains 20 natural proteins selected from UniProt (Consortium, 2022), with lengths ranging from approximately 50 to 350 amino acids. The UniProt identifiers and lengths of the 20 targets are listed in Table 3. The second target is the SARS-CoV-2 spike protein, included as an additional long sequence. SARS-CoV-2 spike is a high-impact and widely studied antigen in COVID-19 vaccine development, and is commonly used as a representative long target; structurally, the SARS-CoV-2 spike glycoprotein is a major focus of vaccine research and a primary target of host immune defenses (Bangaru et al., 2020).

5.2. Baselines

For each target protein \mathbf{p} , we compare our designed sequence against baselines produced by LinearDesign (Zhang et al., 2023) and EnsembleDesign (Dai et al., 2025). For each baseline method, we use the output sequence produced by its official implementation as the representative baseline for that target. All baseline sequences and our sequences are re-evaluated under the same scoring pipeline described below to ensure a fair comparison.

5.3. Scoring Pipeline and Decoding Settings.

All structure-informed metrics are evaluated under a consistent thermodynamic parameter set and decoding configuration. Specifically, MFE is evaluated with LinearFold -V -d0 -b100, and EFE/AUP/AccessU are evaluated with LinearPartition -V -d0 -b100. Here -V selects the ViennaRNA energy parameter set to ensure all methods are scored under the same thermodynamic model, and -d0 disables dangle-energy contributions. The beam size -b100 applies beam pruning to accelerate evaluation. For CAI evaluation in SARS-CoV-2 spike experiments, we use the human codon-usage frequency table as the reference.

5.4. Optimization Settings.

We optimize lattice logits θ using the sample–evaluate–update procedure in Section 4, with Adam updates in logit space (Eq. (26)). We use Adam with $(\beta_1, \beta_2) = (0.9, 0.999)$, and set the initial learning rate to $\eta = 0.1$ in all experiments. Each iteration samples a batch of M sequences from the current lattice distribution and evaluates the target objective on each sample.

5.5. Initialization of the Sampling Distribution.

The initial lattice distribution is constructed by mixing a LinearDesign-based distribution with a uniform distribution. Concretely, for each lattice state s , we initialize the local transition distribution as

$$p_{\theta_1}(\cdot | s) = \epsilon p_{\theta_{\text{LD}}}(\cdot | s) + (1 - \epsilon) p_{\theta_{\text{unif}}}(\cdot | s), \quad (30)$$

where $p_{\theta_{\text{LD}}}(\cdot | s)$ corresponds to the LinearDesign solution projected onto the lattice, and $p_{\theta_{\text{unif}}}(\cdot | s)$ assigns equal probability to all outgoing edges in $\mathcal{A}(s)$. The mixing coefficient $\epsilon \in [0, 1]$ controls the trade-off between initializing near the LinearDesign solution and maintaining exploration. Unless otherwise stated, we set $\epsilon = 0.5$ in all experiments. We then set logits θ_1 such that the softmax in Eq. (14) matches the mixture in Eq. (30) at every state.

5.6. Stopping Criterion and Output Selection.

Our method includes a patience-based early stopping rule (Section 4.4) that terminates optimization when the best objective value has not improved for P consecutive iterations. In principle, this criterion reduces runtime by avoiding unnecessary iterations once the optimization has converged.

In the main experiments reported in this section, however, we adopt a fixed iteration budget T_{\max} for each target and objective. This choice is motivated by the stochasticity of sampling-based optimization: because each iteration is driven by a finite batch, the best-so-far value can exhibit occasional minute improvements even after the optimization has effectively stabilized, which may lead to run-to-run variability in the stopping time under purely automatic early stopping. To obtain comparable compute budgets across targets and baselines and to reduce the sensitivity of termination to stochastic fluctuations, we select T_{\max} based on preliminary convergence curves (objective value versus iteration), choosing a conservative

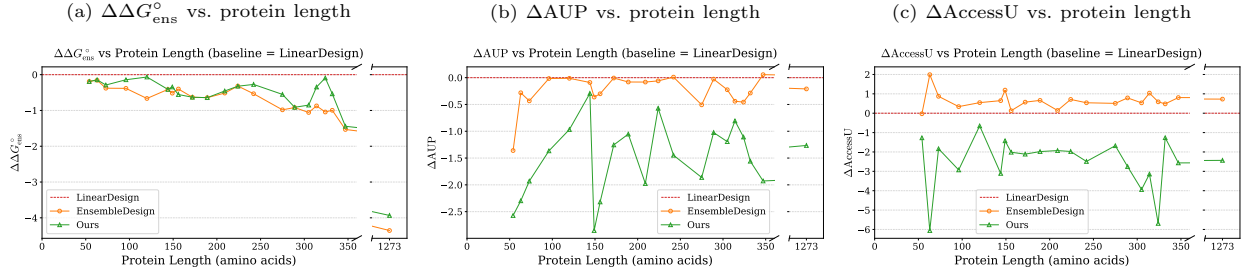


Table 3. Single-metric optimization results across protein sequences. This table compares LinearDesign, EnsembleDesign, and our method on the UniProt set and the SARS-CoV-2 spike protein. For each protein, we report three metrics of the designed mRNA sequence: EFE (denoted $\Delta G_{\text{ens}}^{\circ}$), AUP, and AccessU, all computed under the shared scoring pipeline in Section 5. The LinearDesign block reports absolute metric values for its designed sequence. The EnsembleDesign block reports metric differences relative to LinearDesign, $\Delta(\cdot) \triangleq (\cdot)_{\text{ED}} - (\cdot)_{\text{LD}}$. The **Ours** block is also reported as differences relative to LinearDesign, but it aggregates three single-metric runs with distinct objectives (EFE, AUP, and AccessU), and thus yields one optimized sequence per objective. The last three columns report the corresponding relative changes for the objective optimized in each run, indicated by $*$.

UniProt Proteins											
		LinearDesign (LD)			EnsembleDesign (vs. LD)			Ours (vs. LD)			
ID	length (aa / nt)	$\Delta G_{\text{ens}}^{\circ}$	AUP	AccessU	$\Delta\Delta G_{\text{ens}}^{\circ}$	ΔAUP	$\Delta\text{AccessU}$	$\Delta\Delta G_{\text{ens}}^{\circ*}$	ΔAUP^*	$\Delta\text{AccessU}^*$	
Q13794	54 / 162	-113.39	20.64	2.33	-0.19	-1.36	-0.03	-0.19	-2.57	-1.27	
Q9UI25	63 / 189	-126.07	25.87	6.46	-0.15	-0.28	1.99	-0.14	-2.30	-6.06	
Q9BZL1	73 / 219	-114.87	27.81	2.70	-0.38	-0.43	0.87	-0.29	-1.93	-1.83	
P60468	96 / 288	-234.36	16.80	4.36	-0.38	-0.02	0.34	-0.14	-1.37	-2.93	
Q9NWD9	120 / 360	-226.36	22.62	0.94	-0.67	-0.01	0.55	-0.07	-0.97	-0.65	
P14555	144 / 432	-275.06	18.99	3.63	-0.41	-0.09	0.65	-0.41	-0.29	-3.11	
Q8N111	149 / 447	-335.89	21.86	1.55	-0.52	-0.36	1.19	-0.34	-2.85	-1.42	
P63125	156 / 468	-299.18	22.01	2.71	-0.40	-0.30	0.13	-0.55	-2.32	-2.01	
Q6XD76	172 / 516	-427.19	15.94	2.42	-0.63	-0.01	0.57	-0.63	-1.25	-2.11	
P0DMU9	189 / 567	-361.48	21.83	2.53	-0.64	-0.08	0.66	-0.64	-1.05	-1.98	
P0DPF6	209 / 627	-545.55	14.73	2.25	-0.51	-0.08	0.14	-0.46	-1.98	-1.93	
Q9HD15	224 / 672	-532.98	15.02	2.26	-0.32	-0.06	0.71	-0.32	-0.57	-1.98	
Q6T310	242 / 726	-504.29	16.74	3.40	-0.53	0.01	0.54	-0.27	-1.45	-2.49	
Q9BRP0	275 / 825	-586.50	17.42	2.41	-0.98	-0.51	0.51	-0.55	-1.86	-1.68	
P56178	289 / 867	-606.58	19.00	3.31	-0.92	-0.03	0.79	-0.91	-1.02	-2.75	
Q8NH87	305 / 915	-572.37	17.15	7.03	-1.06	-0.22	0.54	-0.85	-1.19	-3.94	
Q8NGU1	314 / 942	-612.55	16.58	6.77	-0.87	-0.44	1.04	-0.35	-0.81	-3.14	
Q8NGC9	324 / 972	-582.39	21.08	9.93	-1.04	-0.46	0.59	-0.09	-1.11	-5.69	
Q99729	332 / 996	-667.21	22.79	2.02	-1.00	-0.29	0.48	-0.54	-1.56	-1.26	
Q9P2M1	347 / 1041	-663.54	22.08	3.83	-1.53	0.06	0.81	-1.44	-1.93	-2.56	

SARS-CoV-2 spike Protein											
		LinearDesign (LD)			EnsembleDesign (vs. LD)			Ours (vs. LD)			
ID	length (aa/nt)	$\Delta G_{\text{ens}}^{\circ}$	AUP	AccessU	$\Delta\Delta G_{\text{ens}}^{\circ}$	ΔAUP	$\Delta\text{AccessU}$	$\Delta\Delta G_{\text{ens}}^{\circ*}$	ΔAUP^*	$\Delta\text{AccessU}^*$	
SPIKE	1273 / 3819	-2511.49	17.43	3.84	-4.35	-0.21	0.73	-2.47	-1.26	-2.43	

Fig. 2. Single-Metric Optimization on UniProt Proteins and SARS-CoV-2 spike. (a-c) Metric change relative to LinearDesign (baseline = 0) versus protein length: (a) $\Delta\Delta G_{\text{ens}}^{\circ}$ (EFE), (b) ΔAUP , and (c) $\Delta\text{AccessU}$. In each subfigure: red baseline: LinearDesign; Orange curve: EnsembleDesign–LinearDesign; green curve: Ours–LinearDesign. Table 3 Detailed breakdown: LinearDesign reports metric values of its sequence; EnsembleDesign and Ours report differences relative to LinearDesign.

cutoff after which further iterations yield negligible improvement on average. We still track the best-so-far sequence throughout the run and report the final output as

$$\mathbf{x}^* \triangleq \underset{\mathbf{x} \text{ sampled during the run}}{\operatorname{argmin}} F(\mathbf{x}, \mathbf{p}), \quad (31)$$

i.e., the best-scoring sampled sequence under the optimized objective.

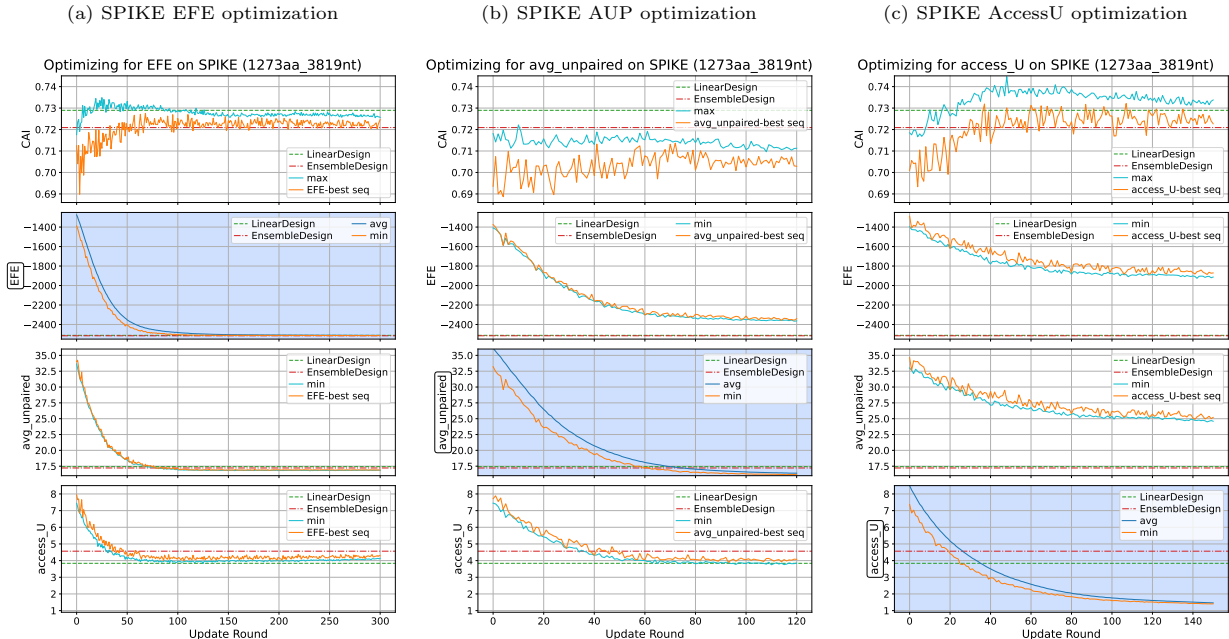


Fig. 3. SARS-CoV-2 spike trajectories for single-metric optimization. Panels (a)–(c) correspond to optimizing EFE, AUP, and AccessU on the spike protein, respectively. Each panel contains trajectories of sampled-sequence statistics over iterations. Subplots with blue backgrounds indicate the primary optimized metric. In a primary-metric subplot, the blue curve denotes the batch mean over sampled sequences, and the orange curve denotes the value of the best sampled sequence under the corresponding optimization objective. In the remaining subplots, the orange curve reports the other metric values of that same best-by-objective sampled sequence, and the cyan curve denotes the best sampled value of that metric within each batch.

6. Evaluation Results

6.1. Single-Metric Optimization

We first evaluate our method under three single-metric objectives by optimizing EFE, AUP, and AccessU separately. All sequences are scored using the shared evaluation pipeline in Section 5. Figure 2(a–c) summarizes how the achieved metric values change with protein length, reported as differences relative to the LinearDesign baseline (thus LinearDesign appears at 0). In each panel, the orange curve shows EnsembleDesign relative to LinearDesign, and the green curve shows our method relative to LinearDesign.

Optimizing EFE. Figure 2(a) reports $\Delta\Delta G_{\text{ens}}^{\circ}$ versus protein length. We use batch size $M = 500$, with $T_{\text{max}} = 50$ iterations for UniProt and $T_{\text{max}} = 300$ iterations for SARS-CoV-2 spike. Across protein targets, our method yields a consistent reduction in EFE relative to LinearDesign. Compared with EnsembleDesign, our EFE values are typically slightly higher (worse), but the gap is small on most proteins, and there exist targets where our design matches or surpasses EnsembleDesign.

Optimizing AUP. Figure 2(b) reports ΔAUP versus protein length. We use batch size $M = 500$, with $T_{\text{max}} = 80$ iterations for UniProt and $T_{\text{max}} = 120$ iterations for SARS-CoV-2 spike. Here the advantage of our method is pronounced: the green curve remains consistently below both baselines across the UniProt set and on SARS-CoV-2 spike, indicating substantially lower AUP. Notably, this

improvement is maintained as length increases, suggesting that the sample–evaluate–update procedure scales well for driving down global unpairedness, rather than relying on idiosyncratic gains on short sequences.

Optimizing AccessU. Figure 2(c) reports $\Delta\text{AccessU}$ versus protein length. We use batch size $M = 500$, with $T_{\text{max}} = 80$ iterations for UniProt and $T_{\text{max}} = 150$ iterations for SARS-CoV-2 spike. Our method achieves consistently lower AccessU than both LinearDesign and EnsembleDesign across all protein targets. For most targets, we achieve improvements exceeding 1%.

SARS-CoV-2 spike optimization trajectories and cross-metric effects. In addition, Fig. 3(a)–(c) further illustrates the optimization dynamics on the spike protein when EFE, AUP, and AccessU are optimized separately as single objectives. Our method updates the parameters of the sampling lattice, so these plots show how sequence-level statistics obtained from lattice samples evolve over iterations, rather than the trajectory of a single sequence.

Overall, all three single-objective runs improve their primary objective, while also exhibiting clear cross-metric coupling effects. When optimizing EFE, AUP also decreases noticeably as a byproduct, indicating that under the current folding model, shifting the lattice distribution toward lower-EFE regions simultaneously biases sampling toward sequences with lower unpaired probability. Conversely, when optimizing AUP, EFE also improves to a non-negligible extent. This bidirectional

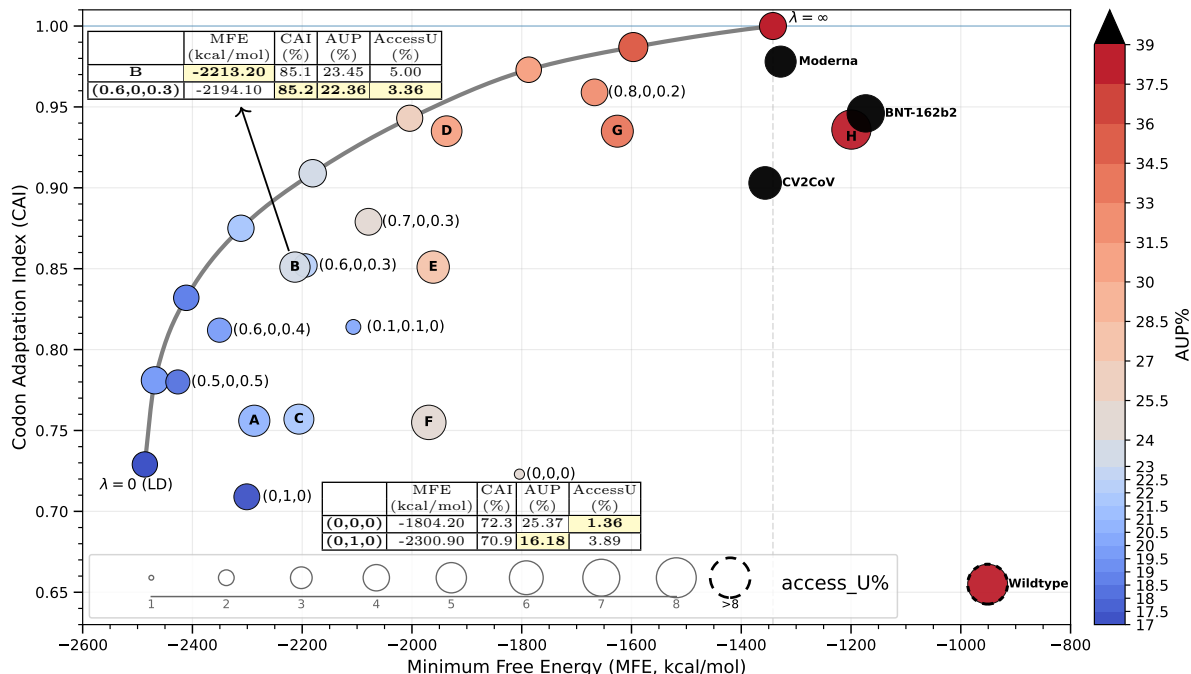


Fig. 4. Comparison of COMBO optimization on SARS-CoV-2 spike with prior designs in the LinearDesign design space. The spike mRNA design space is visualized in four dimensions: minimum free energy (MFE; x-axis) and codon adaptation index (CAI; y-axis), with point color encoding AUP (percent; colorbar) and circle size encoding AccessU (percent; size legend). The gray curve is the feasibility limit (optimal boundary) computed by LinearDesign by varying the codon-optimality weight λ from 0 to ∞ . Points A–G are spike sequences designed by LinearDesign as suboptimal candidates, and H is a codon-optimized baseline designed by OptimumGene. Four reference SARS-CoV-2 spike mRNA sequences are annotated for comparison: *Wildtype*, *BNT-162b2*, *mRNA-1273 (Moderna)*, and *CV2CoV*. COMBO results are shown as points labeled by (α, β, δ) , where $(\alpha, \beta, \gamma, \delta)$ satisfy $\alpha, \beta, \gamma, \delta \geq 0$ and $\alpha + \beta + \gamma + \delta = 1$ (thus $\gamma = 1 - \alpha - \beta - \delta$).

behavior suggests a strong association between EFE and AUP in our experimental setting.

In contrast, AccessU optimization shows a different byproduct pattern: compared with optimizing EFE or AUP, optimizing AccessU leads to a more pronounced improvement in CAI. This is reasonable because reducing AccessU can in part be achieved by decreasing the U content of the sequence, which in turn changes the synonymous-codon usage distribution and can indirectly increase CAI.

6.2. COMBO-Metric Optimization

Figure 4 places our COMBO-optimized SARS-CoV-2 spike designs into the same MFE–CAI design space used by LinearDesign (Zhang *et al.*, 2023), augmented with AUP (color) and AccessU (circle size). By adjusting the weight tuple (α, β, δ) (with $\gamma = 1 - \alpha - \beta - \delta$), the optimization can be steered toward different trade-offs within the spike design space, providing a practical mechanism to select sequences that prioritize different metrics. All COMBO runs use batch size $M = 200$ with the fixed $T_{\max} = 350$ iterations.

Comparison to published reference sequences. Relative to the wild type spike coding sequence, the COMBO designs shown in Fig. 4 achieve simultaneous improvements across all four displayed metrics. Compared

with widely used reference designs, including BNT-162b2, mRNA-1273 (Moderna), CV2CoV, and the codon-optimized baseline H, the setting $(\alpha, \beta, \delta) = (0.8, 0, 0.2)$ produces a competitive design that improves MFE, AUP, and AccessU relative to these references, with CAI only slightly below mRNA-1273.

Weight-controlled trade-offs and examples of movement in the design space. Two single-metric extremes are also visible: $(0, 1, 0)$ emphasizes AUP optimization, whereas $(0, 0, 0)$ corresponds to emphasizing AccessU via $\gamma = 1$. Starting from $(0, 0, 0)$, adding modest weight to CAI and AUP yields $(0.1, 0.1, 0)$, improving CAI, MFE, and AUP while only slightly sacrificing AccessU. Along a different direction, decreasing α while increasing δ (with $\beta = 0$ and $\gamma = 1 - \alpha - \delta$) induces a systematic shift in the MFE–CAI plane: the sequence $(0.8, 0, 0.2) \rightarrow (0.7, 0, 0.3) \rightarrow (0.6, 0, 0.4) \rightarrow (0.5, 0, 0.5)$ moves leftward toward lower MFE while gradually reducing CAI, forming a smooth trade-off curve that follows the general direction of the LinearDesign feasibility boundary. Notably, $(0.6, 0, 0.3)$ lies close to the LinearDesign sequence B in the MFE–CAI plane, while achieving better CAI, AUP, and AccessU with only a small trade-off in MFE (with the gains in AUP and AccessU each exceeding 1%).

7. Conclusions

We introduced sampling-based continuous optimization framework for synonymous mRNA design that leverages a parameterized lattice representation of the synonymous space $\mathcal{X}(\mathbf{p})$. By placing trainable logits θ on local lattice transitions, the method induces a distribution $p_{\theta}(\mathbf{x})$ supported only on feasible coding sequences, and optimizes the expected objective via an iterative sample–evaluate–update procedure.

In single-metric experiments, our method reliably drives down the targeted objective across the UniProt set and the SARS-CoV-2 spike protein under a shared scoring pipeline. Most notably, when optimizing AUP or AccessU, our designed sequences achieve lower values than both LinearDesign and EnsembleDesign, demonstrating a consistent advantage in reducing global unpairedness and U-accessibility.

In COMBO optimization, the explicit weight $(\alpha, \beta, \gamma, \delta)$ enables weight-controlled navigation of the multi-objective design space: by tuning these coefficients, we can select design sequences that satisfy different optimization preferences and occupy different regions of the design space (e.g., trading off stability and codon optimality). Importantly, the framework is extensible: additional computable metrics can be incorporated into $F(\mathbf{x}, \mathbf{p})$, allowing our approach to optimize richer objective combinations beyond the current metric set.

References

- Baden, L. R., Sahly, H. M. E., Essink, B., Kotloff, K., Frey, S., Novak, R., Diemert, D., Spector, S. A., Roupael, N., Creech, C. B., McGettigan, J., Khetan, S., Segall, N., Solis, J., Brosz, A., Fierro, C., Schwartz, H., Neuzil, K., Corey, L., Gilbert, P., Janes, H., Follmann, D., Marovich, M., Mascola, J., Polakowski, L., Ledgerwood, J., Graham, B. S., Bennett, H., Pajon, R., Knightly, C., Leav, B., Deng, W., Zhou, H., Han, S., Ivarsson, M., Miller, J. and Zaks, T. (2021). Efficacy and Safety of the mRNA-1273 SARS-CoV-2 Vaccine. *New England Journal of Medicine*, **384**(5), 403–416.
- Bangaru, S., Ozorowski, G., Turner, H. L., Antanasijevic, A., Huang, D., Wang, X., Torres, J. L., Diedrich, J. K., Tian, J.-H., Portnoff, A. D., Patel, N., Massare, M. J., Yates, J. R., Nemazee, D., Paulson, J. C., Glenn, G., Smith, G. and Ward, A. B. (2020). Structural analysis of full-length SARS-CoV-2 spike protein from an advanced vaccine candidate. *Science*, **370**(6520), 1089–1094.
- Consortium, T. U. (2022). UniProt: the Universal Protein Knowledgebase in 2023. *Nucleic Acids Research*, **51**(D1), D523–D531.
- Dai, N., Zhou, T., Tang, W. Y., Mathews, D. H. and Huang, L. (2025). EnsembleDesign: messenger RNA design minimizing ensemble free energy via probabilistic lattice parsing. *Bioinformatics*, **41**(Supplement_1), i391–i400.
- Greensmith, E., Bartlett, P. L. and Baxter, J. (2004). Variance reduction techniques for gradient estimates in reinforcement learning. *Journal of Machine Learning Research*, **5**(Nov), 1471–1530.
- Huang, L., Zhang, H., Deng, D., Zhao, K., Liu, K., Hendrix, D. A. and Mathews, D. H. (2019). LinearFold: linear-time approximate RNA folding by 5′-to-3′ dynamic programming and beam search. *Bioinformatics*, **35**(14), i295–i304.
- Kingma, D. P. and Ba, J. (2017). Adam: A method for stochastic optimization.
- Krueger, R. K. and Ward, M. (2025). JAX-RNAfold: scalable differentiable folding. *Bioinformatics*, **41**(5), btaf203.
- Leppek, K., Byeon, G. W., Kladwang, W., Wayment-Steele, H. K., Kerr, C. H., Xu, A. F., Kim, D. S., Topkar, V. V., Choe, C., Rothschild, D., Tiu, G. C., Wellington-Oguri, R., Fujii, K., Sharma, E., Watkins, A. M., Nicol, J. J., Romano, J., Tunguz, B., Diaz, F., Cai, H., Guo, P., Wu, J., Meng, F., Shi, S., Participants, E., Dormitzer, P. R., Solórzano, A., Barna, M. and Das, R. (2022). Combinatorial optimization of mRNA structure, stability, and translation for RNA-based therapeutics. *Nature Communications*, **13**(1), 1536.
- Polack, F. P., Thomas, S. J., Kitchin, N., Absalon, J., Gurtman, A., Lockhart, S., Perez, J. L., Marc, G. P., Moreira, E. D., Zerbini, C., Bailey, R., Swanson, K. A., Roychoudhury, S., Koury, K., Li, P., Kalina, W. V., Cooper, D., Frenck, R. W., Hammitt, L. L., Özlem Türeci, Nell, H., Schaefer, A., Ünal, S., Tresnan, D. B., Mather, S., Dormitzer, P. R., Şahin, U., Jansen, K. U. and Gruber, W. C. (2020). Safety and Efficacy of the BNT162b2 mRNA Covid-19 Vaccine. *New England Journal of Medicine*, **383**(27), 2603–2615.
- Sharp, P. M. and Li, W.-H. (1987). The codon adaptation index—a measure of directional synonymous codon usage bias, and its potential applications. *Nucleic Acids Research*, **15**(3), 1281–1295.
- Tang, W. Y., Dai, N., Zhou, T., Mathews, D. H. and Huang, L. (2026). SamplingDesign: RNA Design via Continuous Optimization with Coupled Variables and Monte-Carlo Sampling. *Nature Communications (to appear)*.
- Williams, R. J. (1992). Simple statistical gradient-following algorithms for connectionist reinforcement learning. *Machine Learning*, **8**(3), 229–256.
- Zhang, H., Zhang, L., Mathews, D. H. and Huang, L. (2020). Linearpartition: linear-time approximation of rna folding partition function and base-pairing probabilities. *Bioinformatics*, **36**(Supplement_1), i258–i267.
- Zhang, H., Zhang, L., Lin, A., Xu, C., Li, Z., Liu, K., Liu, B., Ma, X., Zhao, F., Jiang, H., Chen, C., Shen, H., Li, H., Mathews, D. H., Zhang, Y. and Huang, L. (2023). Algorithm for optimized mRNA design improves stability and immunogenicity. *Nature*, **621**(7978), 396–403.